Available online at www.sciencedirect.com

ScienceDirect

journal homepage: www.elsevier.com/locate/he

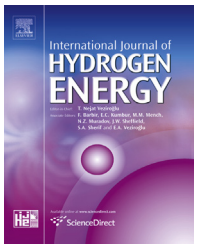

Photoelectrocatalytic properties of $BiVO_4$ prepared with different alcohol solvents

Francisco Wirley Paulino Ribeiro [a], *Murilo Fernando Gromboni* [a], *Frank Marken* [b], *Lucia H. Mascaro* [a,*]

[a] *Department of Chemistry, Federal University of São Carlos, Rod. Washington Luiz, km 235, 13565-905, São Carlos, SP, Brazil*

[b] *Department of Chemistry, University of Bath, BA2 7AY, Bath, United Kingdom*

ARTICLE INFO

Article history:
Received 18 April 2016
Received in revised form
15 July 2016
Accepted 18 July 2016
Available online 6 August 2016

Keywords:
$BiVO_4$
Alcohol solvent
Crystal growth
Photoelectrocatalysis
Water splitting

ABSTRACT

$BiVO_4$ has been receiving attention for applications in photoelectrochemical devices. This paper describes the effect of different alcohol solvents (ethanol, ethylene-glycol, PEG300 and PEG 400) on the morphology, crystal growth, crystalline size, thickness, photophysical and photoelectrochemical properties of $BiVO_4$ photoanodes prepared from a suitable, simple and inexpensive one-step process. All samples exhibited good crystallinity with the monoclinic phase dominating and with suitable bandgap for visible light harvesting; but the morphology, thickness, and resulting photocurrents varied broadly. The unmodified $BiVO_4$ photoanode prepared with PEG 300, gave a particularly good photocurrent of 0.77 mA cm^{-2} at 1.23 V *vs* RHE under illumination of 100 mW cm^{-2}. In this case, a higher value for the ratio between the intensities of the XRD peaks, (040)/(121), was verified, as well as smaller crystallite size. Considering the type of solvent, the $BiVO_4$ photoanode prepared with PEG 300 exhibited a more intense photocurrent. The optimization of the solvent employed in the synthesis of the $BiVO_4$ photoanode is a crucial step in the development of a photoelectrochemical device based on this material.

Introduction

Photoelectrochemical systems for water splitting technologies could become important components in the renewable energy sector [1,2]. Solar energy can be converted to stored chemical energy, for example, in the form of hydrogen generated from water when applying light to suitable semiconductor electrodes [3,4,5]. Therefore, the preparation of photocathodes and photoanodes based on semiconductor materials with appropriate band-gap energy is important to increase the efficiency of energy conversion driven by sunlight [6,7]. Monoclinic $BiVO_4$ is a well-known and suitable anode material for water splitting devices. It has a valence band energy that is more positive than the potential for water oxidation, good chemical stability in aqueous media, low toxicity, high photoelectrochemical activity and the advantage of visible radiation absorption; it is also composed of earth-abundant elements. Thus, $BiVO_4$ has improved performance when compared to other UV-absorbers, such as traditional TiO_2 semiconductor materials [8–11]. Recently, Monfort et al. have reported that a nanocrystalline $BiVO_4$ photoanode produces a high quantity of hydrogen under simulated solar light (100 mW cm^{-2}) when compared to the TiO_2 photoanode [10].

* *Corresponding author.*
E-mail address: lmascaro@ufscar.br (L.H. Mascaro).

http://dx.doi.org/10.1016/j.ijhydene.2016.07.159

The monoclinic phase of $BiVO_4$ is an n-type semiconductor with a valence band dominated by the 6s and 2p orbitals of Bi and O, respectively. The band gap energy for this material is between 2.4 and 2.5 eV and, therefore, it is suitable for sunlight absorption [12,13]. $BiVO_4$ photoanodes have been prepared by several methods such as chemical vapor deposition [14], metal-organic decomposition [15], spray pyrolysis [16], electrostatic spray pyrolysis [17], drop-casting [18], spin coating [19] solution chemical deposition [20], electrodeposition [21], polymer-assisted deposition [22], and electrophoretic deposition [23]. To prepare $BiVO_4$, the precursor reactants are usually applied from aqueous media. In some reports, the addition of polyol solvents such as ethylene-glycol and polyethylene-glycol (PEG) is employed [24–26]. For example, Eda et al. prepared $BiVO_4$ powder from precursors in a nitric acid solution containing PEG-200 [24]. Addullah et al. dissolved salts of Bi and V in ethyleneglycol and obtained the $BiVO_4$ photocatalyst for the removal of methylene blue [25]. The preparation of $BiVO_4$ immobilized on silica fibers with ethanol/nitric acid as solvent was proposed by Wu et al. [26].

The preparation of a $BiVO_4$ photoanode using only alcohol-based solvents was considered in two recent reports [18,27]. Depending on the reaction conditions, these solvents can act as morphology-directing agents. They are inexpensive organics with a stabilizing effect on colloids, they allow for simple synthetic procedures and may promote adherence, homogeneity and transparency of the obtained photoanode films [18,28,29]. According to Zhang et al., both the large number of hydrogen-bonds possible between extended PEG molecular chains and the strong coordination of oxygen with metal cations contribute to the formation of thermodynamically stable solutions, resulting in nanoparticles with high surface activity [30]. He et al. proposed the synthesis of $BiVO_4$ nanoflake films on FTO substrates by drop casting from a metal precursor solution prepared in ethylene-glycol and PEG 600, followed by drying and annealing at 500 °C for 2.5 h [18]. Recently, Mascaro et al. prepared a nanostructured $BiVO_4$ film on ITO substrates by deposition from a metal precursor dispersed in PEG300, followed by annealing at 500 °C for 1 h [27]. Despite the simplicity and advantages of this methodology, we have not found any previous studies in the literature focused on the comparison of different types of alcohol to improve the photoelectrochemical properties of $BiVO_4$. Thus, the aim of this paper is to synthesize and characterize $BiVO_4$ photoanodes prepared from precursor metal solutions containing different alcohol-based solvents, such as ethanol, ethylene-glycol, PEG300 and PEG 400, in order to elucidate the morphology-directing effects and the resulting photoelectrochemical activity of such materials.

Experimental

Reagents

The precursor reagents used to prepare $BiVO_4$ were $Bi(NO_3)_3 \cdot 5H_2O$, NH_4VO_3, ethanol, ethylene-glycol, PEG300 and PEG400 (Sigma–Aldrich). All chemicals were of analytical grade and were used without further purification. The ultrapure water (18.2 MΩ/cm) was produced by a Milli–Q Simplicity 185 system (Millipore).

$BiVO_4$ photoanode preparation

The photo-electrodes were prepared following a slightly modified procedure compared to the one previously published [27]. Precursor solutions were prepared by dissolving a suitable amount of the reagents in each alcohol solvent. Thus, 0.207 g mL^{-1} and 0.050 g mL^{-1} of $Bi(NO_3)_3 \cdot 5H_2O$ and NH_4VO_3, respectively, were separately prepared in 2.5 mL of each alcohol, followed by sonication in an ultrasound bath for 30 min. Then, both solutions were mixed and sonicated again for 30 min. Next, 15 μL of the resulting solution was drop cast on a previously cleaned FTO electrode substrate (surface area, 1.5 cm^2) and the resulting material was heated at 180 °C for 40 min to obtain a homogeneous film. This procedure was performed twice to increase the thickness and uniformity of the film. Finally, the monoclinic phase of $BiVO_4$ was obtained by annealing at 500 °C for 1 h in an open tube furnace.

Characterization

The crystalline phase of $BiVO_4$ was characterized by X-ray diffraction (XRD) using a Shimadzu diffractometer model XRD-6000 in θ–2θ mode, from 10° to 80° with a rate of 2 deg min^{-1} and an electrode voltage of 30 kV. Micro-Raman measurements were made with a Horiba Jobin Yvon (HR 550) system with a 514.5 nm wavelength incident argon laser light coupled with an optical microscope (Olympus BX41). The morphology and thickness of the films were evaluated by high-resolution field emission scanning electron microscopy (FE-SEM, Zeiss Supra 35 at 2 kV). The band gap energy (E_g) values for the $BiVO_4$ photoanodes were calculated from UV–vis diffuse reflectance spectroscopy (DRS) data obtained with a Cary 5 E spectrometer, with the wavelength operating from 200 to 800 nm. The E_g values were calculated using the following equations [31].

$$\alpha = F(R) = (1-R)^2 \Big/ 2R \text{ and } (\alpha h\nu)^2 = A(h\nu - E_g) \quad (1)$$

Here α is the absorption coefficient, F(R) is the Kubelka-Munk function, R is the absolute reflectance for a given hν, h is the Planck constant, ν is the frequency of light and A is a constant. The variable n is a parameter that depends on the interband transition, assuming 2 or 2/3 for direct (allowed and forbidden, respectively) and 1/2 or 1/3 for indirect transitions (allowed and forbidden, respectively).

Photoelectrochemical measurements

Photoelectrochemical measurements were performed with a potentiostat/galvanostat (Autolab PGSTAT 302N, Metrohm-Eco Chemie) using GPES and FRA 4.9 software and with illumination from a 50–500 W Xenon spectrum solar simulator (Newport, 66902). A conventional three-electrode electrochemical cell with quartz windows was used. The reference electrode was Ag/AgCl in saturated KCl, the auxiliary electrode was a platinum plate, and the working electrode was a $BiVO_4$/FTO photoanode. The simulated sunlight for

photoanode illumination was of about 100 mW cm^{-2} (1 sun) with the AM 1.0 filter. Linear scan voltammetry (LSV) experiments were carried out at 20 mV s^{-1} with 0.5 mol L^{-1} Na_2SO_4 (pH = 5.4) as supporting electrolyte. Photoelectrodes were illuminated from the front or back side. The potential scale conversion from *vs* Ag/AgCl to *vs* reversible hydrogen electrode (RHE) was made using Eq. (2).

$$E(vs\ RHE) = E(vs\ Ag/AgCl) + 0.199\ V + 0.0591\ pH \quad (2)$$

Potentiodynamic electrochemical impedance spectroscopy experiments conducted at a 1 kHz in the dark condition were employed in order to estimate both the flat band potential (E_{fb}) and the charge carriers density (N_D) values. This is possible using the Mott–Schottky equation [13,32,33].

$$1/C^2 = 2/\varepsilon\varepsilon_0 A^2 e N_D (E - E_{fb} - k_B T/e) \quad (3)$$

Here C is the space charge capacitance of the semiconductor, ε is the dielectric constant of the semiconductor (68 for $BiVO_4$) [12], ε_0 is the vacuum permittivity, A is the surface area, *e* is the electronic charge, *E* is the applied potential, *k* is the Boltzmann constant and T represents the absolute temperature. The E_{fb} is calculated from the x-intercept on the potential axis after subtracting kT/*e*, which is negligible at room temperature. The N_D can be estimated from the slope of the straight line of the Mott–Schottky graph.

Results and discussion

Characterization of the $BiVO_4$ photoanodes

Initially, XRD measurements were performed to characterize the crystalline phase of $BiVO_4$/FTO photoanode films produced from different alcohol solvents. Fig. 1 shows the XRD data for all $BiVO_4$ films on FTO substrates.

All $BiVO_4$/FTO photoanode films showed good crystallization. All of the characteristic diffraction peaks for the monoclinic phase of $BiVO_4$ were present in each case, with the face (121) at $2\theta = 29°$ being more intense for all solvents, as showed in Fig. 1(A). Furthermore, the characteristic diffraction peak at 24° for zircon-tetragonal phase was not observed in the XRD pattern in Fig. 1(A). According to Kho et al., temperatures higher than 360 °C produce high crystallinity and, above 430 °C, the monoclinic $BiVO_4$ phase is obtained [34]. Therefore, the temperature of 500 °C applied for 1 h is suitable for the formation of crystalline $BiVO_4$.

The (011), (110) and (040) facets are the most important to the photocatalytic activity for splitting water to form O_2 and H_2 [35,36]. The evaluation of the intensity ratios between diffraction peaks can be used to compare growth orientation preferential effects. Fig. 1(B) shows the ratio between intensities for the XRD peaks (011)/(121), (110)/(121) and (040)/(121) for different solvents. All ratios decreased when PEG 400 solvent was used, suggesting that, in this case, the growth of each one of the more photoactive facets was inhibited. The ratios were dependent on the type of solvent, suggesting that preferential growth of crystalline planes happened when the solvent was changed. The peak for the FTO substrate at 26.5° was observed mainly in the samples prepared with ethanol and PEG300, probably due to increased porosity or reduced thickness.

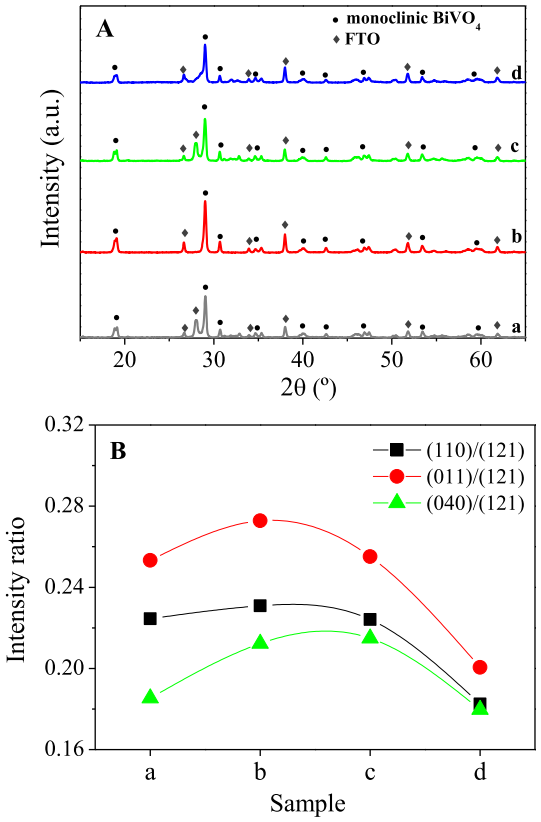

Fig. 1 – (A) XRD patterns for $BiVO_4$/FTO prepared with ethanol (a), ethylene-glycol (b), PEG 300 (c), and PEG 400 (d). (B) Ratio between intensities of the XRD peaks (011)/(121), (110)/(121) and (040)/(121) for $BiVO_4$.

Raman spectra for $BiVO_4$ photoanode films prepared with different alcohol solvents and FTO substrates are shown in Fig. 2.

All spectra display an intense vibrational band around 835 cm^{-1} that can be assigned to symmetric stretching of the

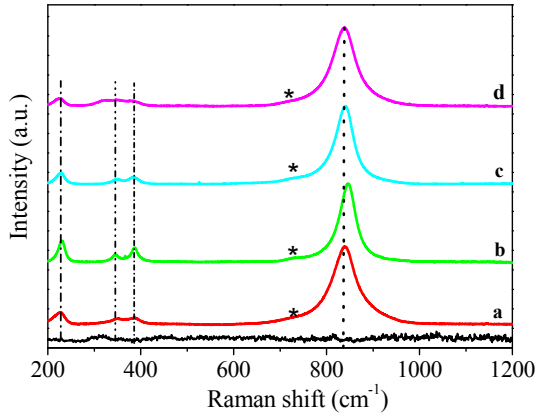

Fig. 2 – RAMAN spectra of $BiVO_4$/FTO obtained using ethanol (a), ethylene-glycol (b), PEG 300 (c), and PEG 400 (d) solvents.

V–O bond (A_g symmetry) [35]. Other typical bands for $BiVO_4$ were observed around 227 cm^{-1}, external mode, and also around 330 and 380 cm^{-1}, described for asymmetric and symmetric bending mode of the VO_4 tetrahedron, respectively [37,38]. Although less intense, a band was also observed around 720 cm^{-1}, indicative of the asymmetric stretching mode of the VO_4 tetrahedron. The monoclinic phase for $BiVO_4$ usually has stretching modes for V–O in the range 826–832 cm^{-1} [37]. The shift towards higher wavenumbers observed for all $BiVO_4$ photoanode films can be attributed to a V–O bond length decrease in the monoclinic phase. Hardcaster et al. showed that the length of the V–O bond can be estimated using the following equation [39].

$$\nu(cm^{-1}) = 21349 \exp\left[-1.9176\, R(\text{Å})\right] \quad (4)$$

Here ν is the Raman shift for the V–O symmetric stretch and R is the bond length. Considering the Raman shift values observed in the spectra shown in Fig. 2, the average V–O bond lengths are calculated as 1.688 Å ($BiVO_4$/FTO–ethanol), 1.684 Å ($BiVO_4$/FTO–ethylene-glycol), 1.688 Å ($BiVO_4$/FTO–PEG300) and 1.689 Å ($BiVO_4$/FTO–PEG400), which are in agreement with the reported value (1.69 Å) for the length of the V–O bond in the monoclinic Scheelite phase of $BiVO_4$ [40]. The differences in the bond lengths can be attributed to differences in particle morphology.

SEM images of $BiVO_4$ films can be seen in Fig. 3. All $BiVO_4$ films exhibit distinct porous surfaces. Ethanol and PEG 300 seem to give more porous films whereas the ethylene-glycol based film appears more uniform and finer. PEG 400 resulted in the presence of aggregates over the surface decreasing the porosity; this is impairs the penetration of the solution. Besides, the electron/hole recombination process can still be favorable in the $BiVO_4$ photoanode prepared with PEG 400. The porous structure eases the penetration of the electrolyte solution and the inter-particle connection is important for electron transfer in the semiconductor [41]. Therefore, a finer-grained and denser morphology could be beneficial.

The cross-sectional images reveal that the thickness of the $BiVO_4$ films on the FTO substrate was strongly dependent on the solvents. The preparation method resulted in a porous $BiVO_4$ film well attached to the FTO substrate. Fig. 4 shows the relationships between the thickness values and the alcohol solvents. The thicknesses in the order of micrometers are due to the drop casting procedure for dispersing the $BiVO_4$ precursor solution over the FTO substrate.

Increased thickness was observed for the film obtained with ethanol, with values of about 8 μm. This can be attributed to the rapid elimination of the ethanol solvent in the annealing step because of its higher vapor pressure when compared to the other solvents. Ethylene-glycol, PEG300 and PEG400 seem to result in a decrease in the thickness of the $BiVO_4$ film.

In the cross-sectional images, it can also be observed that the $BiVO_4$ film prepared with ethanol showed regions distributed with empty space and flaws in the contact between the $BiVO_4$ particles and the FTO substrate. In this case, the photogenerated charge transport between particles and the electron transfer to the FTO could be minimized, resulting in lower photocurrent response. However, ethylene-glycol and PEG solvents provided good contact between $BiVO_4$ and the FTO substrate; in addition, the film obtained with PEG 400 had fewer pores when compared to the one obtained with PEG

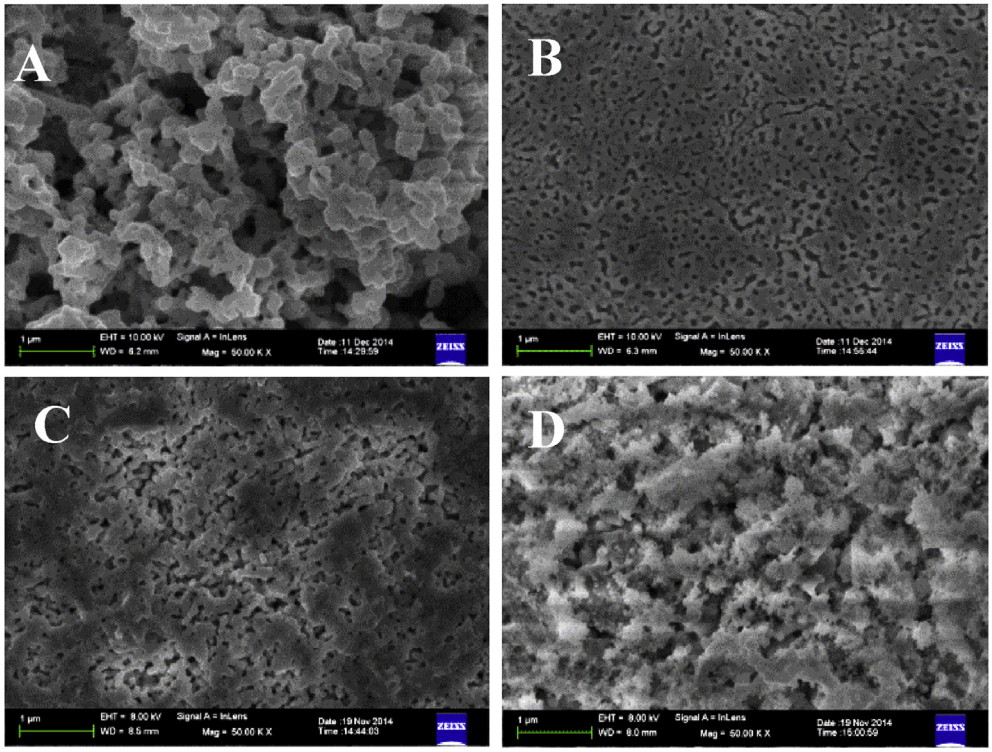

Fig. 3 – SEM images of $BiVO_4$/FTO obtained in ethanol (A), ethylene-glycol (B), PEG300 (C), and PEG400 (D).

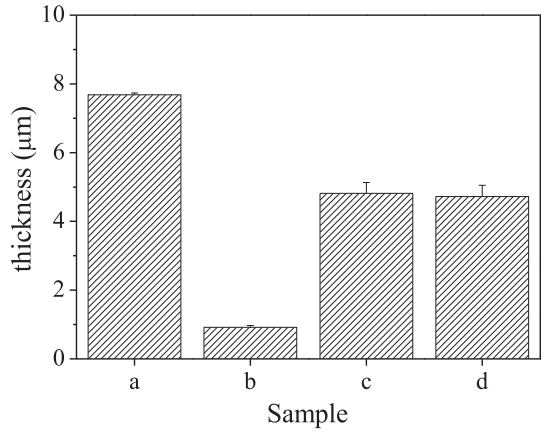

Fig. 4 – Relationship between thickness and the solvent applied during the synthesis of the $BiVO_4$ film: ethanol (a), ethylene-glycol (b), PEG300 (c), and PEG400 (d).

300. The $BiVO_4$ film was compact and uniformly porous with particle size of around 350 nm in the case of the PEG 300 solvent. The most compact film was observed for the $BiVO_4$ film prepared with ethylene-glycol, explaining its lower porosity; this result is in agreement with the SEM images shown in Fig. 3.

Photophysical proprieties of $BiVO_4$ films

The photophysical properties of the photoanode films were investigated by UV–vis-DRS. Fig. 5 shows the UV–vis diffuse reflectance spectra of $BiVO_4$ prepared with different alcohol solvents.

All films showed the characteristic absorption of monoclinic $BiVO_4$ in the visible light region. The band gap (E_g) for different $BiVO_4$ photoanode films was calculated as described in the Experimental Section. $BiVO_4$ has an allowed direct transition (n = 2). Therefore, E_g values were estimated by extrapolation employing the linear relationship between $(\alpha h\nu)^2$ and $h\nu$. The calculated values ranged from 2.46 to 2.69 eV. Similar values for the $BiVO_4$ semiconductor were reported previously [24,34]. The lowest values were obtained when the PEG300 solvent was used; the values were 2.46 eV and 2.48 eV for PEG300 and PEG400, respectively. According to the literature, the monoclinic phase has E_g in the range 2.4–2.5 eV [12]. Thus, band gap data seems independent of the type the PEG solvents studied. A similar value (E_g = 2.44 eV) was obtained when PEG200 was employed in $BiVO_4$ synthesis [24]. An increase was observed when using other alcohol solvents with lower molecular mass, with E_g values of 2.51 and 2.58 for $BiVO_4$ photoanode films prepared with ethylene-glycol and ethanol, respectively. The difference could be associated with factors such as change of particle and crystallite sizes, morphology, coupled oxides and defects [42–44]. Despite the differences in the E_g values, it has been reported that for visible-light harvesting the band gap of the semiconductor should be narrower than 3.0 eV [6].

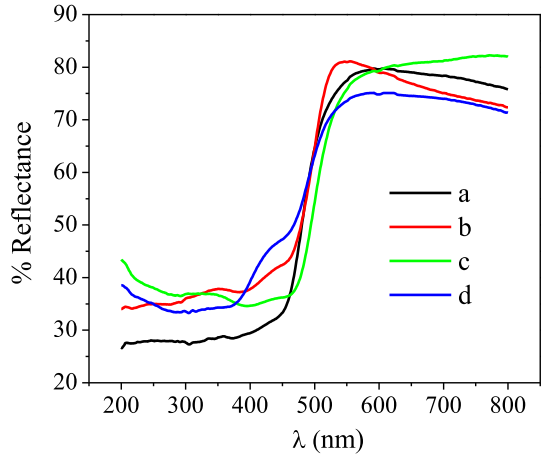

Fig. 5 – UV–Vis diffuse reflectance of $BiVO_4$/FTO electrodes obtained in ethanol (a), ethylene-glycol (b), PEG300 (c), and PEG400 (d).

Photoelectrochemical measurements

The photoelectrochemical measurements with front-side and back-side illumination were performed in 0.5 mol L^{-1} Na_2SO_4, pH 5.4, using LSV in a potential range from −0.5 to 1.55 V at 20 mV s^{-1} for $BiVO_4$/FTO obtained with different alcohol solvents. As expected, the photocurrent onset potentials, in 0.5 mol L^{-1} Na_2SO_4, for all $BiVO_4$ photoanodes, were much lower compared to that for the bare FTO substrate (Table 1).

The shift to lower potentials under back-side illumination on $BiVO_4$/FTO photoanode films is due to the photoelectrocatalytic activity of the $BiVO_4$ semiconductor in the presence of visible light. In all cases, the photocurrent was more intense for back-side illumination in comparison with front-side illumination, in agreement with a strong light absorption by $BiVO_4$. This behavior has been reported as a result of the slow electron carrier transport from the $BiVO_4$/solution interface to the electric contact [13,16]. Furthermore, the recombination process under back-side illumination has a lower probability when compared to front-side illumination, due to the fast trap-free electron diffusion in the vicinity of the FTO [45]. Fig. 6(A) shows the linear voltammograms obtained for the photoanode under back-side illumination with light on/off for each $BiVO_4$/FTO.

For all photoanodes, the presence of spikes with the light on/off change was observed due to recombination in the surface of the semiconductor. When the overpotential increased, the transient spikes decreased significantly; such behavior can be associated with a decrease of the energy loss attributed to recombination processes [46].

According to Xiao et al., the correlation between photocurrent and thickness is only possible if the particle sizes are similar and uniform. In this case, the film with thickness above 450 nm showed differences in the photocurrent obtained from back and front side illumination, because it is outside the region of thickness in which light absorbance dominates the photocurrent [45]. Furthermore, $BiVO_4$ films with thickness from 550 nm showed similar back-side illumination photocurrents. However, in our

Table 1 – Flat-band potential (E_{fb}), charge carriers density (N_D), onset potential of the FTO substrate and $BiVO_4$/FTO photoanode films.

Photoanode	*E_{onset} (V) *vs* Ag/AgCl	E_{fb} (V) *vs* Ag/AgCl	N_D (cm^{-1})
FTO	0.87	$-1.07 \pm 5.80 \times 10^{-2}$	$1.82 \pm 0.14 \times 10^{21}$
$BiVO_4$/FTO – a	0.26	$-0.62 \pm 1.01 \times 10^{-2}$	$5.64 \pm 0.38 \times 10^{19}$
$BiVO_4$/FTO – b	−0.03	$-0.65 \pm 0.84 \times 10^{-2}$	$4.75 \pm 0.73 \times 10^{19}$
$BiVO_4$/FTO – c	0.03	$-0.75 \pm 1.90 \times 10^{-2}$	$3.47 \pm 0.47 \times 10^{19}$
$BiVO_4$/FTO – d	0.04	$-0.76 \pm 0.72 \times 10^{-2}$	$3.19 \pm 0.33 \times 10^{19}$

With a(ethanol), b(ethylene-glycol), c(PEG 300) and d(PEG 400).
*Back side illumination.

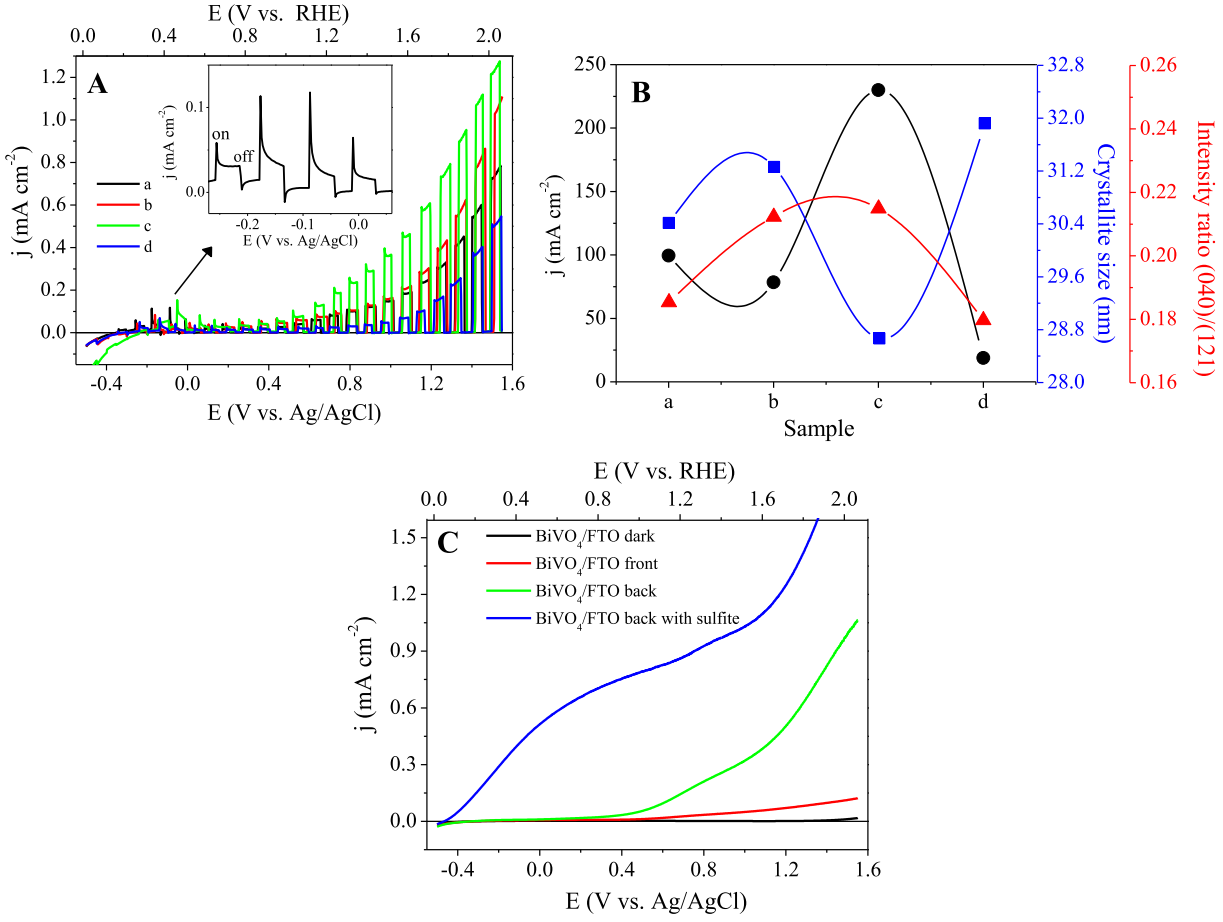

Fig. 6 – (A) LSVs for $BiVO_4$/FTO prepared with ethanol (a), ethylene-glycol (b), PEG300 (c), and PEG400 (d). Insert: spikes in photocurrent with the light on/off. (B) Comparison of photocurrent, XRD intensity ratios between the peaks (040)/(121), and crystallite sizes of $BiVO_4$ samples prepared with different solvents. (C) LSV without and with Na_2SO_3 for $BiVO_4$/FTO prepared with PEG300 at 20 mV s^{-1}.

studies, the back-side photocurrent was dependent on the alcohol solvent used in the synthesis; these results can be attributed to changes in the morphology and particle sizes of the $BiVO_4$, influencing hole diffusion and electron collection. The highest photocurrent intensity was obtained for $BiVO_4$/FTO photoanodes produced with PEG300. This can be attributed to the morphology and density of the $BiVO_4$ films. It can be concluded that a finer, uniformly porous film can facilitate the generation of the electron/hole pair and the penetration of solution, allowing the interfacial water oxidation reaction:

$$2H_2O_{(l)} + 4\ \text{holes}\left(4\ h^+\right) \rightarrow O_{2(g)} + 4H^+(aq) + 4e^- \quad (5)$$

Fig. 6(B) shows the relationship between photocurrent density, crystallite size estimated by Scherrer equation and the ratio between the diffraction peaks (040)/(121) for different solvents employed in the $BiVO_4$ synthesis. The results showed that the highest photocurrent value was observed at the

highest (040)/(121) ratio and smaller crystallite size, both observed for PEG 300.

Fig. 6(C) shows the linear voltammograms obtained in 0.5 mol L^{-1} Na_2SO_4, without and with 0.5 mol L^{-1} Na_2SO_3 acting as a hole scavenger, in a potential range from −0.5 to 1.55 V at 20 mV s^{-1} for $BiVO_4$/FTO obtained with PEG300. As can be observed in Fig. 6(B), the presence of Na_2SO_3 increased the photocurrent due to the fast oxidation kinetics when water oxidation is considered. The photoelectrochemical response was typical of the presence of the hole scavenger. The photocurrent at 1.23 V *vs* RHE, converted using the relationship as described in the Experimental section, was 0.230 mA cm^{-2} and 0.775 mA cm^{-2}, in presence and absence of 0.5 mol L^{-1} Na_2SO_3, respectively.

According to the literature, different photocurrent values are reported for the $BiVO_4$ photoanode at the standard reversible redox potential for water oxidation (1.23 V *vs* RHE). Rettie et al., reported the synthesis of epitaxial and polycrystalline $BiVO_4$ by pulsed laser deposition promoting photocurrents of about 0.15 and 0.05 mA cm^{-2} in 0.1 mol L^{-1} Na_2SO_4, with and without 0.1 mol L^{-1} Na_2SO_3, respectively [44]. According to Brack et al., $BiVO_4$ prepared by aerosol-assisted chemical vapor deposition exhibited 0.400 mA cm^{-2} in 1.0 mol L^{-1} Na_2SO_4 [14]. Electrosprayed $BiVO_4$ showed a photocurrent of 0.230 mA cm^{-2} in 0.5 mol L^{-1} Na_2SO_4 [47]. Electrostatic spray pyrolysis was applied to prepare $BiVO_4$ nanoparticles; the photoelectrochemical response obtained was about 0.350 mA cm^{-2} in 0.5 mol L^{-1} Na_2SO_4 [17]. He et al. described a method with two steps based in Bi electrodeposition in the presence of Zn^{2+} ions, which act as a directing agent, followed by chemical-thermal process; a photocurrent of about 1.0 mA cm^{-2} in 0.1 mol L^{-1} phosphate buffer solution was observed [48]. $BiVO_4$/β-$Bi_4V_2O_{11}$ obtained by spray pyrolysis showed a photoelectrochemical response of 0.09 mA cm^{-2} in 0.5 mol L^{-1} Na_2SO_4 [49]. Monfort et al. described the synthesis of $BiVO_4$ with the surfactant triton X-100 as structure control agent. The photoelectrochemical response was investigated in different aqueous electrolytes. In this case the photocurrent was about 0.650 mA cm^{-2} in 0.5 mol L^{-1} $NaHCO_3$ [10]. Despite the application of alcohol solvents such as PEG, the literature is very scarce. According to He et al., the photocurrent response of nanoflake $BiVO_4$ prepared with PEG600 was about 0.3 mA cm^{-2} (1.23 V *vs* RHE). However, in the same work when $BiVO_4$ was doped with W and Co, the photocurrent increases to about 1.0 mA cm^{-2} and 1.8 mA cm^{-2}, without and with a hole scavenger (Na_2SO_3), respectively [26]. According to Mascaro et al., the photocurrent was 0.120 mA cm^{-2} (1.23 V vs RHE) for $BiVO_4$ prepared with PEG300 [27]. Therefore, the photocurrent values for the $BiVO_4$ samples prepared in the present work were very close to values previously published, showing that the use of PEG is an interesting alternative to prepare photoanodes. Moreover, the optimization of the solvent applied for the synthesis of the $BiVO_4$ photoanode is a crucial step in the development of photoelectrochemical devices based on this material, because in the best conditions, the addition of agents, catalysts or dopants, can improve the efficiency of the photoanodes. The photocurrent value is also dependent on a set of parameters, such as morphology, dopant, catalytic materials and heterojunctions with other oxides [8,9,18,50–54]. Recently, Liu et al. have proposed the synthesis of Cu-doped $BiVO_4$. In this case, $BiVO_4$ containing Cu with gradient doping concentration profile was synthesized by depositing a CuO layer between $BiVO_4$ and FTO followed by annealing. The photoelectrochemical response obtained was about 0.100 mA cm^{-2} in Na_2SO_4 0.5 mol L^{-1} [51]. According Xie et al., the $BiVO_4$, Mo:$BiVO_4$ and NiO/Mo:$BiVO_4$ p–n junctions exhibited photocurrent values of about 0.050, 0.150 and 0.300 mA cm^{-2} in KH_2PO_4 0.1 mol L^{-1}, respectively [52]. WO_3/$BiVO_4$ obtained by the auto-combustion method showed photocurrent of 3.43 mA cm^{-2} in Na_2SO_3 0.5 mol L^{-1} [53].

Furthermore, due to the slower kinetics of water oxidation, the addition of a hole scavenger to the electrolyte solution drastically increases the photocurrent response [55]. For example, a photocurrent of about 4.0 mA cm^{-2} was recently published for $BiVO_4$ with FeOOH/NiOOH dual-layer oxygen evolution catalysts in the presence of a hole scavenger (Na_2SO_3 1 mol L^{-1}) [56]. In addition, heterojunctions based in core–shell nanowire WO_3/W:$BiVO_4$ and core–shell WO_3/$BiVO_4$ + CoPi exhibited high photocurrent, 3.1 mA cm^{-2} and 6.7 mA cm^{-2}, respectively [50,57].

The repeatability of the photoelectrochemical response of the developed $BiVO_4$/FTO photoanode (PEG300) was evaluated by two sets of experiments. Initially, 7 measurements were performed by LSV with 20 mV s^{-1} in 0.5 mol L^{-1} Na_2SO_4 under back-side illumination. Before each experiment, the solution was mechanically stirred. In this condition, the calculated relative standard deviations (RSD) were 6.2% and 1.7% for the potentials of 0.71 V (1.23 V *vs* RHE) and 1.1 V, respectively. Next, continuous LSV experiments were performed and the RSD were 5.5% and 3.2% for the potentials 0.71 V (1.23 V vs ENH) and 1.1 V, respectively. Therefore, the photoelectrochemical device based on $BiVO_4$/FTO prepared with PEG300 presents good repeatability and reproducibility in the photoelectrochemical response.

Fig. 7 shows the chronoamperogram obtained for the $BiVO_4$/FTO photoanode film under front and back-side illumination with an applied potential of 1.1 V *vs* Ag/AgCl.

The value for the photocurrent under back-side illumination was higher. After the onset of light, a fast increase in current was observed, followed by the characteristic decay of

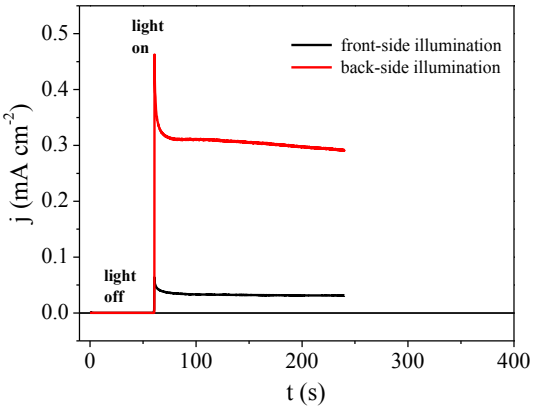

Fig. 7 – Chronoamperograms in 0.5 mol L^{-1} Na_2SO_4 for $BiVO_4$/FTO prepared with PEG 300 under front and back-side illumination at 1.1 V *vs* Ag/AgCl.

photocurrent attributed to characteristic recombination processes for $BiVO_4$ photoanodes. The photocurrent stabilizes around 20 s after the illumination for all photoanodes. The kinetics of charge recombination in semiconductor electrodes can be assessed by a transient time constant (τ) [58]. Initially, the parameter D is calculated according to Eq. (6).

$$D = (I_t - I_s)/(I_m - I_S) \quad (6)$$

Here I_t is the photocurrent at time t, I_s is the steady-state photocurrent, and I_m is the initial photocurrent. As previously reported, the τ value is obtained by finding the time in which $\ln D = -1$ in the relationship between ln D and time [58]. The τ values calculated for the $BiVO_4$/FTO photoanode film under front and back side illumination were 3.3 and 1.9 s, respectively. Thus, the relatively slower recombination process is observed for front side illumination, although these values are very similar.

As can be observed in the insert of Fig. 7, the photocurrent values under back-side illumination were improved for uniformly porous $BiVO_4$/FTO photoanode films (ethanol, ethylene-glycol and PEG300). Therefore, under back-side illumination the photocurrent was dependent on film morphology and porosity. Electrochemical impedance spectroscopy measurements in potentiodynamic mode were carried out at 1 kHz in 0.5 mol L^{-1} Na_2SO_4, pH 5.4, for $BiVO_4$/FTO photoanode films in order to obtain the flat band potential (E_{fb}) and charge carriers density (N_D) by Mott–Schottky analyses. Table 1 lists the E_{fb} and N_D values obtained for the FTO substrate and for $BiVO_4$/FTO photoanode films prepared with different solvents. The profile of the Mott–Schottky plots obtained for all samples showed the characteristic behavior for n-type semiconductors with slope $\partial C^{-2}/\partial E > 0$ [32]. The E_{fb} and N_D values calculated for the FTO substrate were −1.07 V (−0.55 V *vs* RHE) and $1.82 \pm 0.14 \times 10^{21}$ cm^{-3}, respectively. The calculated E_{fb} values ranged from −0.62 to −0.76 V *vs* Ag/AgCl (−0.10 to −0.24 V *vs* RHE). These E_{fb} values were more negative than was observed for the onset potential of photocurrents that appeared in the linear voltammetry experiments. The E_{fb} is similar to the Fermi level when the band is flat (no bending, no electric field) and is always close to the conduction band edge in an n-type semiconductor [59]. The N_D values calculated by the slope of the Mott–Schottky plots ranged from $3.19 \pm 0.33 \times 10^{19}$ to $6.82 \pm 0.47 \times 10^{19}$ cm^{-3} for $BiVO_4$/FTO photoanode films. It is important to note that the charge carrier density is not necessarily associated with the increase of photocurrent intensity. For example, in the present study the highest photocurrent intensity was observed for $BiVO_4$/FTO prepared with PEG300 ($N_D = 3.47 \pm 0.47 \times 10^{19}$ cm^{-3}). Looking at all the evidence from the comparison of the photoelectrochemical properties of the films, it appears that the better performance of the PEG300-derived photoanode films cannot be simply linked to physical parameters and that grain sizes, morphology and porosity also need to be considered.

Conclusions

$BiVO_4$ semiconductor films were successfully deposited onto FTO substrates based on a rapid one-step procedure employing different alcohol solvents (ethanol, ethylene-glycol, PEG300 and PEG 400). All samples exhibited the monoclinic Scheelite phase and bandgap energy in the range from 2.46 to 2.69 eV, satisfactory for visible light harvesting as previously reported in literature for $BiVO_4$ photoanode films. However, different morphologies, crystal growths, crystallite sizes and thicknesses were obtained for the $BiVO_4$ films, depending on the type of precursor solvent, with significant effects on the photocurrents. The voltammograms with the light on/off exhibited the characteristic spikes attributed the recombination process. All photoanodes showed more intense photocurrent under back-side illumination when compared to front-side. Moreover, the photocurrent under back-side was dependent on the alcohol solvent as indicative of the differences in morphology and particle size. The most interesting $BIVO_4$/FTO photoanode film in terms of photoelectrochemical activity was obtained with PEG300. This was the best solvent for the synthesis of $BiVO_4$ films. The photocurrent density values obtained in 0.5 mol L^{-1} Na_2SO_4 with and without 0.5 mol L^{-1} Na_2SO_3, at 1.23 V *vs* RHE, were 0.230 mA cm^{-2} and 0.775 mA cm^{-2}, respectively. Morphology and device performance are sensitive to precursor deposition and further improvements may be possible in future.

Acknowledgements

The authors wish to thank São Paulo Research Foundation (FAPESP) for grants 2014/06704–2 and 2013/07296-2, INCTMN 2008/57872–1, CNPq 573636/2008–7 and CAPES (PVE 71/2013).

REFERENCES

[1] Qureshy AM, Ahmed M, Dincer I. Simulation of transport phenomena in a photoelectrochemical reactor for solar hydrogen production. Int J Hydrogen Energy 2016;41:8020–31. http://dx.doi.org/10.1016/j.ijhydene.2015.12.218.

[2] Juodkazytė J, Seniutinas G, Šebeka B, Savickaja I, Malinauskas T, Badokas K, et al. Solar water splitting: efficiency discussion. Int J Hydrogen Energy 2016;41:11941–8. http://dx.doi.org/10.1016/j.ijhydene.2016.05.079.

[3] Ahmad H, Kamarudin SK, Minggu LJ, Kassim M. Hydrogen from photo-catalytic water splitting process: a review. Renew Sustain Energy Rev 2015;43:599–610. http://dx.doi.org/10.1016/j.rser.2014.10.101.

[4] Choudhary S, Upaddhyay S, Kumar P, Singh N, Satsangi VR, Shrivastav R, et al. Nanostructured bilayered thin films in photoelectrochemical water splitting - a review. Int J Hydrogen Energy 2012;37:18713–30. http://dx.doi.org/10.1016/j.ijhydene.2012.10.028.

[5] Molinari R, Marino T, Argurio P. Photocatalytic membrane reactors for hydrogen production from water. Int J Hydrogen Energy 2014;39:7247–61. http://dx.doi.org/10.1016/j.ijhydene.2014.02.174.

[6] Suarez CM, Hernández S, Russo N. $BiVO_4$ as photocatalyst for solar fuels production through water splitting: a short review. Appl Catal A Gen 2015;504:158–70. http://dx.doi.org/10.1016/j.apcata.2014.11.044.

[7] Gan J, Lu X, Tong Y. Towards highly efficient photoanodes: boosting sunlight-driven semiconductor nanomaterials for

water oxidation. Nanoscale 2014;6:7142–64. http://dx.doi.org/10.1039/c4nr01181c.
[8] Lichterman MF, Shaner MR, Handler SG, Brunschwing BS, Gray HB, Lewis NS, et al. Enhanced stability and activity for water oxidation in alkaline media with bismuth vanadate photoelectrodes modified with a cobalt oxide catalytic layer produced by atomic layer deposition. J Phys Chem Lett 2013;4:4188–91.
[9] Zhou M, Bao J, Xu Y, Zhang J, Xe J, Guan M, et al. Photoelectrodes based upon Mo:$BiVO_4$ inverse opals for photoelectrochemical water splitting. ACS Nano 2014;8:7088–98.
[10] Monfort O, Pop L, Sfaelou S, Plecenik T, Roch T, Dracopoulos V, et al. Photoelectrocatalytic hydrogen production by water splitting using $BiVO_4$ photoanodes. Chem Eng J 2016;286:91–7. http://dx.doi.org/10.1016/j.cej.2015.10.043.
[11] Lu Y, Shang H, Shi F, Chao C, Zhang X, Zhang B. Preparation and efficient visible light-induced photocatalytic activity of m-$BiVO_4$ with different morphologies. J Phys Chem Solids 2015;85:44–50. http://dx.doi.org/10.1016/j.jpcs.2015.04.016.
[12] Ma Y, Pendlebury SR, Reynal A, Le Formal F, Durrant JR. Dynamics of photogenerated holes in undoped $BiVO_4$ photoanodes for solar water oxidation. Chem Sci 2014;5:2964–73. http://dx.doi.org/10.1039/C4SC00469H.
[13] Park Y, McDonald KJ, Choi K. Progress in bismuth vanadate photoanodes for use in solar water oxidation. Chem Soc Rev 2013;42:2321–37. http://dx.doi.org/10.1039/c2cs35260e.
[14] Brack P, Sagu JS, Peiris TAN, McInnes A, Senili M, Wijayantha KGU, et al. Aerosol-assisted CVD of bismuth vanadate thin film and their photoelectrochemical properties. Chem Vap Depos 2015;21:41–5. http://dx.doi.org/10.1002/cvde.201407142.
[15] Luo W, Wang J, Zhao X, Zhao Z, Li Z, Zou Z. Formation energy and photoelectrochemical properties of $BiVO_4$ after doping at Bi^{3+} or V^{5+} sites with higher valence metal ions. Phys Chem Chem Phys 2013;15:1006–13. http://dx.doi.org/10.1039/c2cp43408c.
[16] Li M, Zhao L, Guo L. Preparation and photoelectrochemical study of $BiVO_4$ thin films deposited by ultrasonic spray pyrolysis. Int J Hydrogen Energy 2010;35:7127–33. http://dx.doi.org/10.1016/j.ijhydene.2010.02.026.
[17] Liu X, Liu Y, Su J, Li M, Guo L. Facile preparation of $BiVO_4$ nanoparticle film by electrostatic spray pyrolysis for photoelectrochemical water splitting. Int J Hydrogen Energy 2015;40:12964–72. http://dx.doi.org/10.1016/j.ijhydene.2015.08.015.
[18] He H, Berglund SP, Rettie AJE, Chemelewski WD, Xiao P, Zhang Y, et al. Synthesis of $BiVO_4$ nanoflake array films for photoelectrochemical water oxidation. J Mater Chem A 2014;2:9371–9. http://dx.doi.org/10.1039/c4ta00895b.
[19] Zhang L, Lin C, Valev VK, Reisner E, Steiner U, Baumberg JJ. Plasmonic enhancement in $BiVO_4$ photonic crystals for efficient water splitting. Small 2014;10:3970–8. http://dx.doi.org/10.1002/smll.201400970.
[20] Dong W, Guo Y, Zhang Y, Li H, Liu H. Photoelectric properties of $BiVO_4$ thin films deposited on fluorine doped tin oxide substrates by a modified chemical solution deposition process. Int J Hydrogen Energy 2014;39:5569–74. http://dx.doi.org/10.1016/j.ijhydene.2014.02.006.
[21] Dall'Antonia LH, De Tacconi NR, Chanmannee W, Temmaji H, Myung N, Rajeshwar K. Electrosynthesis of bismuth vanadate photoelectrodes. Electrochem Solid-State Lett 2010;13:D29–32. http://dx.doi.org/10.1149/1.3322641.
[22] Luo H, Mueller AH, McCkeskey TM, Burrell AK, Bauer E, Jia QX. Structural and photoelectrochemical properties of $BiVO_4$ thin films. J Phys Chem C 2008;112:6099–102. http://dx.doi.org/10.1021/jp7113187.
[23] Zhang Y, Guo Y, Duan H, Li H, Sun C, Liu H. Facile synthesis of V^{4+} self-doped, [010] oriented $BiVO_4$ nanorods with highly efficient visible light-induced photocatalytic activity. Phys Chem Chem Phys 2014;16:24519–26. http://dx.doi.org/10.1039/C4CP03795B.
[24] Eda S, Fujishima M, Tada H. Low temperature-synthesis of $BiVO_4$ nanorods using polyethylene glycol as a soft template and the visible-light-activity for copper acetylacetonate decomposition. Appl Catal B Environ 2012;125:288–93. http://dx.doi.org/10.1016/j.apcatb.2012.05.038.
[25] Abdullah AH, Moey HJM, Yusof NA. Response surface methodology analysis of the photocatalytic removal of methylene blue using bismuth vanadate prepared via polyol route. J Environ Sci 2012;24:1694–701. http://dx.doi.org/10.1016/S1001-0742(11)60966-2.
[26] Wu Q, Chen P, Zhao L, Zhao J, Wu J, Qi X, et al. Photocatalytic behavior of $BiVO_4$ immobilized on silica fiber via a combined alcohol-thermal and carbon nanofibers template route. Cat Commun 2014;49:29–33. http://dx.doi.org/10.1016/j.catcom.2014.02.002.
[27] Mascaro LH, Pockett A, Mitchels JM, Peter LM, Cameron PJ, Celorrio V, et al. One-step preparation of the $BiVO_4$ film photoelectrode. J Solid State Electrochem 2015;19:31–5. http://dx.doi.org/10.1007/s10008-014-2495-y.
[28] Wolcott A, Kuykendall TR, Chen W, Chen S, Zhang JZ. Synthesis and characterization of ultrathin WO_3 nanodisks utilizing long-chain poly(ethylene glycol). J Phys Chem B 2006;110:25288–96. http://dx.doi.org/10.1021/jp064777b.
[29] Hariharan V, Radhakrishnan S, Oarthibavarman M, Dhilipkumar R, Sekar C. Synthesis of polyethylene glycol (PEG) assisted tungsten oxide (WO_3) nanoparticles for l-dopa bio-sensing applications. Talanta 2011;85:2166–74. http://dx.doi.org/10.1016/j.talanta.2011.07.063.
[30] Zhang G, Xu Y, Gao D, Sun Y. α-Fe_2O_3 nanoplates: PEG-600 assisted hydrothermal synthesis and formation mechanism. J Alloys Compd 2011;509:885–90. http://dx.doi.org/10.1016/j.jallcom.2010.09.124.
[31] Nowak M, Kauch B, Szperlich P. Determination of energy band gap of nanocrystalline SbSi using diffuse reflectance spectroscopy. Rev Sci Instrum 2009;80. http://dx.doi.org/10.1063/1.3103603. 046107–3.
[32] Gelderman K, Lee L, Donne SW. Flat-band potential of a semiconductor: using the Mott-Schottky equation. J Chem Educ 2007;84:685–8. http://dx.doi.org/10.1021/ed084p685.
[33] Liu C, Yang Y, Li W, Li J, Li Y, Chen Q. Construction of novel Bi_2S_3 nanobelt @ WO_3 nanoplate arrays on FTO glass with high photoelectrochemical activity. Int J Hydrogen Energy 2016;41:5878–86. http://dx.doi.org/10.1016/j.ijhydene.2016.01.171.
[34] Kho YK, Teoh WY, Iwase A, Mädler L, Kudo A, Amal R. Flame preparation of visible-light-responsive $BiVO_4$ oxygen evolution photocatalysts with subsequent activation via aqueous route. ACS Appl Mater Interfaces 2011;3:1997–2004. http://dx.doi.org/10.1021/am200247y.
[35] Wang D, Jiang H, Zong X, Xu Q, Ma Y, Li G, et al. Crystal facet dependence of water oxidation on $BiVO_4$ sheets under visible light irradiation. Chem Eur J 2011;17:1275–82. http://dx.doi.org/10.1002/chem.201001636.
[36] Kim HR, Kim G, In S, Park Y. Optimization of porous $BiVO_4$ photoanode from electrodeposited Bi electrode: structural factors affecting photoelectrochemical performance. Electrochim Acta 2016;189:252–8. http://dx.doi.org/10.1016/j.electacta.2015.12.106.
[37] Merupo V, Velumani S, Ordon K, Errien N, Szade J, Kassiba A. Structural and optical characterization of ball-milled copper-doped bismuth vanadium oxide ($BiVO_4$). CrystEngComm 2015;17:3366–75. http://dx.doi.org/10.1039/C5CE00173K.

[38] Xue Y, Wang X. The effects of Ag doping on crystalline structure and photocatalytic properties of $BiVO_4$. Int J Hydrogen Energy 2015;40:5878–88. http://dx.doi.org/10.1016/j.ijhydene.2015.03.028.
[39] Hardcastle FD, Wachs IE. Determination of vanadium-oxygen bond distances and bond orders by Raman spectroscopy. J Phys Chem 1991;95:5031–41. http://dx.doi.org/10.1021/j100166a025.
[40] Tokuganaga S, Kato H, Kudo A. Selective preparation of monoclinic and tetragonal $BiVO_4$ with scheelite structure and their photocatalytic properties. Chem Mater 2001;13:4624–8. http://dx.doi.org/10.1021/cm0103390.
[41] Kim ES, Kang HJ, Magesh G, Kim JY, Jang J, Lee JS. Improved photoelectrochemical activity of $CaFe_2O_4/BiVO_4$ heterojunction photoanode by reduced surface recombination in solar water oxidation. ACS Appl Mater Interfaces 2014;6:17762–9. http://dx.doi.org/10.1021/am504283t.
[42] Shang M, Wang W, Zhou L, Sun S, Yin W. Nanosized $BiVO_4$ with high visible-light-induced photocatalytic activity: ultrasonic-assisted synthesis and protective effect of surfactant. J Hazard Mater 2009;172:338–44. http://dx.doi.org/10.1016/j.jhazmat.2009.07.017.
[43] Qi X, Zhu X, Wu J, Wu Q, Li X, Gu M. Controlled synthesis of $BiVO_4$ with multiple morphologies via an ethylenediamine-assisted hydrothermal method. Mater Res Bull 2014;59:435–41. http://dx.doi.org/10.1016/j.materresbull.2014.08.004.
[44] Rettie AJE, Mozaffari S, McDaniel MD, Pearson KN, Ekerdt JG, MArkert JT, et al. Pulsed laser deposition of epitaxial and polycrystalline bismuth vanadate thin films. J Phys Chem C 2014;118:26543–50. http://dx.doi.org/10.1021/jp5082824.
[45] Xiao S, Chen H, Yang Z, Long X, Wang Z, Zhu Z, et al. Origin of the different photoelectrochemical performance of mesoporous $BiVO_4$ photoanodes between the $BiVO_4$ and the FTO side illumination. J Phys Chem C 2015;119:23350–7. http://dx.doi.org/10.1021/acs.jpcc.5b07505.
[46] Wang G, Ling Y, Wang H, Xirong L, Li Y. Chemically modified nanostructures for photoelectrochemical water splitting. J Photochem Photobiol C-Photochem Rev 2014;19:35–51. http://dx.doi.org/10.1016/j.jphotochemrev.2013.10.006.
[47] Yoon H, Mali MG, Chon JY, Kim M, Choi SK, Park H, et al. Nanotextured pillars of electrosprayed bismuth vanadate for efficient photoelectrochemical water splitting. Langmuir 2015;3:3727–37. http://dx.doi.org/10.1021/acs.langmuir.5b00486.
[48] He W, Wang R, Zhou C, Yang J, Li F, Xiang X. Controlling the structure and photoelectrochemical performance of $BiVO_4$ photoanodes prepared from electrodeposited bismuth precursors: effect of zinc ions as directing agent. Ind Eng Chem Res 2015;54:10723–30. http://dx.doi.org/10.1021/acs.iecr.5b02460.
[49] Dos Santos WS, Almeida LD, Afonso AS, Rodriguez M, Mesquita JP, Monteiro DS, et al. Photoelectrochemical water oxidation over fibrous and sponge-like $BiVO_4/\beta$-$Bi_4V_2O_{11}$ photoanodes fabricated by spray pyrolysis. Appl Catal B Environ 2016;182:247–56. http://dx.doi.org/10.1016/j.apcatb.2015.09.034.
[50] Rao PM, Cai L, Liu C, Cho IS, Lee CH, Weisse JM. Simultaneously efficient light absorption and charge separation in $WO_3/BiVO_4$ core/shell nanowire photoanode for photoelectrochemical water oxidation. Nano Lett 2014;14:1099–105. http://dx.doi.org/10.1021/nl500022z.
[51] Liu C, Li X, Su J, Guo L. Enhanced charge separation in copper incorporated $BiVO_4$ with gradient doping concentration profile for photoelectrochemical water splitting. Int J Hydrogen Energy 2016;41:12842–51. http://dx.doi.org/10.1016/j.ijhydene.2016.06.068.
[52] Xie S, Zhai T, Zhu Y, Li W, Qiu R, Tong Y, et al. NiO decorated Mo:$BiVO_4$ photoanode with enhanced visible-light photoelectrochemical activity. Int J Hydrogen Energy 2014;39:4820–7. http://dx.doi.org/10.1016/j.ijhydene.2014.01.072.
[53] Fujimoto I, Wang N, Saito R, Miseki Y, Gunji T, Sayama K. $WO_3/BiVO_4$ composite photoelectrode prepared by improved auto-combustion method for highly efficient water splitting. Int J Hydrogen Energy 2014;39:2454–61. http://dx.doi.org/10.1016/j.ijhydene.2013.08.114.
[54] Jiang J, Wang M, Li R, Ma L, Guo L. Fabricating CdS/$BiVO_4$ and $BiVO_4$/CdS heterostructured film photoelectrodes for photoelectrochemical applications. Int J Hydrogen Energy 2013;38:13069–76. http://dx.doi.org/10.1016/j.ijhydene.2013.03.057.
[55] Ribeiro FWP, Moares FC, Pereira EC, MArken F, Mascaro LH. New application for the $BiVO_4$ photoanode: a photoelectroanalytical sensor for nitrite. Electrochem Commun 2015;61:1–4. http://dx.doi.org/10.1016/j.elecom.2015.09.022.
[56] Kim TW, Choi K. Nanoporous $BiVO_4$ photoanodes with dual-layer oxygen evolution catalysts for solar water splitting. Science 2014;343:990–4. http://dx.doi.org/10.1126/science.1246913.
[57] Pishosh Y, Turkevych I, Mawatari K, Uemura J, Kazoe Y, Kosar S, et al. Photocatalytic generation of hydrogen by core-shell $WO_3/BiVO_4$ nanorods with ultimate water splitting efficiency. Sci Rep 2015:1–10. http://dx.doi.org/10.1038/srep11141. 11141.
[58] Ng YH, Iwase A, Kudo A, Amal R. Reducing graphene oxide on a visible-light $BiVO_4$ photocatalyst for an enhanced photoelectrochemical water splitting. J Phys Chem Lett 2010;1:2607–12. http://dx.doi.org/10.1021/jz100978u.
[59] Pilli SK, Janarthanan R, Deutsch TG, Furtak TE, Brown LD, Turner JA, et al. Efficient photoelectrochemical water oxidation over cobalt-phosphate (Co-Pi) catalyst modified $BiVO_4$/1D-WO_3 heterojunction electrodes. Phys Chem Chem Phys 2013;15:14723–8. http://dx.doi.org/10.1039/C3CP52401A.